Electron excitation of Na(3S) and Na(3P) atoms to the Na(3D) state

B. Stumpf*
Joint Institute for Laboratory Astrophysics, University of Colorado and National Bureau of Standards, Boulder, Colorado 80309

A. Gallagher
Joint Institute for Laboratory Astrophysics, University of Colorado and National Bureau of Standards, Boulder, Colorado 80309
and Quantum Physics Division, National Bureau of Standards, Boulder, Colorado 80309
(Received 28 February 1985)

The cross sections for electron-impact excitation of Na(3S) and Na(3P) atoms to the 3D state have been measured from threshold to 1000 eV, with ~0.3 eV resolution. The 3P-state atoms are produced in the $m_l=1$, $m_s=\frac{1}{2}$ level by optical excitation, and $3D\rightarrow 3P$ fluorescence is detected at 90° to the quantization axis. The resulting polarization anisotropies are considered, and included along with cascade effects in the high-energy normalizations to the Born approximation. The $3S\rightarrow 3D$ and $3P\rightarrow 3D$ excitation cross sections both rise very abruptly at threshold, and are indistinguishable from a step function with our energy resolution.

I. INTRODUCTION

Electron collisional excitation of atoms has been studied for many transitions, particularly for the group-I and -II metals and noble gases. The initial state of almost all of these transitions has been a fairly strongly bound S state, and hence these measurements encompass a fairly minor portion of all the types of electronic transitions that can be caused by electron collisions. In particular, transitions between excited states introduce many new issues, such as $L\rightarrow L'$ transitions where L and L' are both large, and transitions between and to levels with many neighboring states. Flannery and McCann[1] have carried out an $nL\rightarrow n'L'$ Born calculation for large nL and $n'L'$ values, finding unusual trends that would not easily be inferred from current knowledge of ground-state excitation. Percival and collaborators[2] have carried out calculations of electron collisions for very high n values. Vriens and Smeets[3] and Shuker *et al.*[4] have used scaling arguments to estimate high n cross sections. In addition to a scientific curiosity regarding the unknown, electron collisions with excited states are important in many practical plasmas, particularly in highly excited gases. As an initial look at these issues we have studied here the $3P\rightarrow 3D$ excitation in Na. Here the effective principal quantum numbers of the initial and final states are ~2 and 3, respectively, and both states are relatively well isolated, so this is an initial, small step toward the general $nL\rightarrow n'L'$ problem.

Several laboratories have studied electron collisions with excited atoms.[5–12] Optogalvanic and fluorescence measurements in discharges have obtained information regarding electron collisions with excited states, but not actual cross sections, since a distribution of electron collision energies and several state-to-state processes are involved. Measurements of superelastic ($3P\rightarrow 3S$) electron collisions with Na* have been used by Hertel and collaborators[9] to probe details of this resonance transition, but this transition is (in reverse) the strongly bound $S\rightarrow P$ type of transition that is so often studied. Hanne *et al.*[10] have studied the spin dependence of this same superelastic Na transition. Trajmar and collaborators[11] have similarly probed differential cross section details of the Ba($6P\rightarrow 6S$) transition, by measuring superelastic collisions with excited Ba. Again, this is the reverse of the strongly bound S to P transition, to which it is connected by detailed balance. Bederson and collaborators[12] have measured electron scattering form excited Na. Thus, while the above measurements of electron collisions with excited atoms have obtained a wealth of new information, only some of the optogalvanic measurements are related to the general high $nL\rightarrow n'L'$ problem, and there a mixture of states and electron collision energies is involved. In contrast, the present experiment is not designed to obtain detailed differential cross sections or cross sections for the very high n region, but to obtain the total cross section for a specific $nL\rightarrow n'L'$ transition for higher effective quantum numbers than has previously been probed.

We have utilized the same "optical excitation-function" method that has been used to obtain many ground-state excitation cross sections,[13] with the addition of optically exciting a large fraction of the Na target atoms to the $3P$ state. The Na energy levels and the processes employed in this experiment are shown in Fig. 1. We measure the intensity of $3D$ state fluorescence (819 nm) resulting from the $3P$-state population (laser on versus off) as a function of electron collision energy. After correcting for fluorescence anisotropy and the change in ground-state excitation to the $3D$ state, the resulting relative $3P\rightarrow 3D$ excitation functions are normalized to the Born approximation (BA) at a high energy, where the latter is accurate. However, in the experiment the optically excited Na($3P$) target atoms are not in a statistical mixture of M_L states, so we actually obtain a final cross section that is somewhat dif-

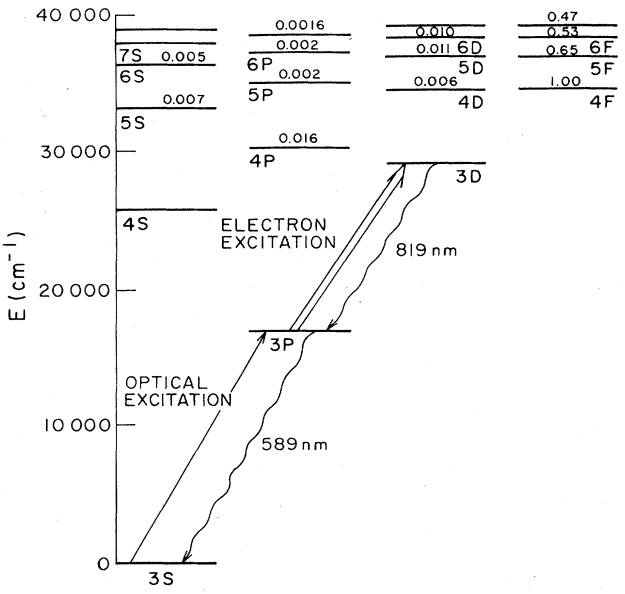

FIG. 1. Na energy levels, the two excitation processes used here to measure the $3P\rightarrow 3D$ cross section, and the two fluorescence wavelengths observed. The numbers above each state are the fraction of the excitation to that state that radiatively cascades into the $3D$ state.

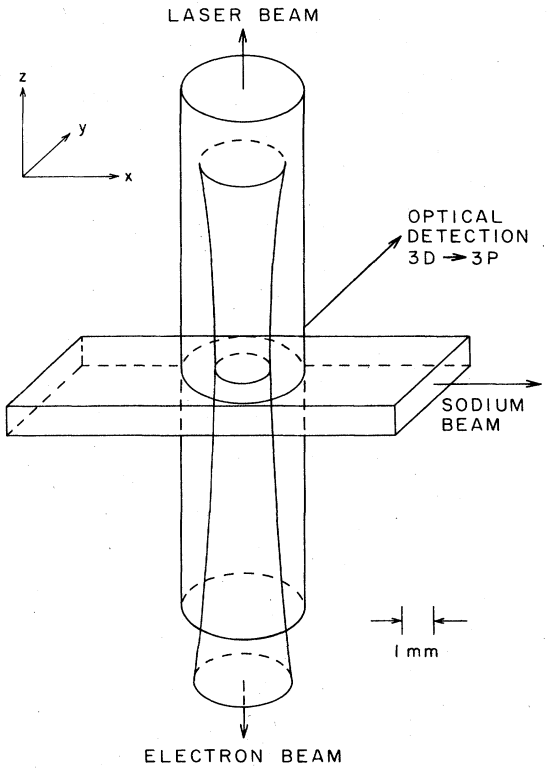

FIG. 2. Diagram of the interaction region, where the three beams overlap. The Na beam is 1.2-mm thick (z direction) and 4.6-mm wide, the circularly polarized laser beam 4 mm in diameter, and the electron beam typically ~ 2 mm in diameter and convergent at $\sim 5°$ half-angle.

ferent than the total cross section for the $3P\rightarrow 3D$ transition. Relations between the measured and total cross section are given here, and more detail will be available from BA calculations in Ref. 14.

II. PRINCIPLE

The experimental arrangement of the interaction region is shown diagramatically in Fig. 2. A sodium beam is intersected at right angles by a cylindrically symmetric electron beam and a counterpropagating, circularly polarized laser beam, tuned to the $F'=2\rightarrow F=3$ hyperfine transition of the $3^2S_{1/2}-3^2P_{3/2}$ (D_2) line (589 nm). Defining the laser beam direction as the z axis, the circularly polarized light pumps sodium atoms into the $F=3$ state with preference to high M_F values. Once stationary conditions are reached, all sodium atoms are either within the two-level system $2S_{1/2}$ $F'=2$, $M_F'=2\leftrightarrow{}^2P_{3/2}$, $F=3$, $M_F=3$ or distributed among the magnetic sublevels of the $F'=1$ ground-state level. This was confirmed by observing that the optically excited resonance fluorescence, observed along y, was fully polarized along the x axis.

Two points are important in defining the atomic target: First, the phase relationship between excited and ground-state atoms, induced by the laser field, need not be considered in the electron excitation since different atoms of the beam have different phases at the instant of electron excitation. Electrons therefore interact with an incoherent mixture of fn excited and $(1-f)n$ ground-state atoms, where f is the excitation fraction and n the total number density of atoms. Second, the excited atoms are in a pure spin and angular momentum state, i.e., the $3^2P_{3/2}$, $F=3$, $M_F=3$ state is a pure $M_L=1$, $M_S=\frac{1}{2}$ state. The excitation cross section of the $3D$ state from this $3P$, $M_L=1$, $M_S=\frac{1}{2}$ state does not depend on the spin orientation M_S, and is given by

$$Q_T(3P,M_L=1,M_S=\tfrac{1}{2}\rightarrow 3D)$$
$$=Q_T(3P,M_L=1\rightarrow 3D)$$
$$=\sum_{M_L'}Q_T(3P,M_L=1\rightarrow 3D,M_L')\ . \quad (1)$$

It is therefore not equivalent to the $3P\rightarrow 3D$ cross section

$$Q_T(3P\rightarrow 3D)=\tfrac{1}{3}[Q_T(3P,M_L=0\rightarrow 3D)$$
$$+2Q_T(3P,M_L=1\rightarrow 3D)]\ . \quad (2)$$

Here we have defined the Q_T as the "total" cross section for state i to state j excitation, including cascades from higher states. We will use Q to indicate direct state i to j excitation cross sections. In both cases these are total cross sections with respect to electron scattering angle. The direct $i\rightarrow 3D$ cross section $Q(i\rightarrow 3D)$ is related to $Q_T(i\rightarrow 3D)$, which includes cascading, by

$$Q_T(i\rightarrow 3D)=Q(i\rightarrow 3D)+\sum_j Q(i\rightarrow j)B(j\rightarrow 3D)\ , \quad (3)$$

where j specifies all states energetically higher than $3D$, and $B(j\rightarrow 3D)$ is the radiation branching ratio from any of these states to $3D$. We detect the light of the $3D\rightarrow 3P$

transition ($\sim$819 nm) emitted perpendicular to the atom and electron beam (I_{90}). This "apparent optical excitation function" I_{90} is related to the isotropically averaged intensity I by the well-known relation $I_{90}=I[3/(3-P)]$, where $P=(I_{\parallel}-I_{\perp})/(I_{\parallel}+I_{\perp})$ is the fluorescence linear polarization.[13] Thus, we define cross sections

$$Q_T(i\rightarrow 3D;90°)=Q_T(i\rightarrow 3D)\frac{3}{3-P_i} . \quad (4)$$

Two $3D\rightarrow 3P$ fluorescence intensity measurements are made. First, with the laser on we measure

$$I_{90°}^{\text{on}}=\kappa n\frac{i}{e_0}l[(1-f)Q_T(3S\rightarrow 3D;90°) + fQ_T(3P,M_L=1,M_S=\tfrac{1}{2}\rightarrow 3D;90°)] \quad (5a)$$

and then, with laser off,

$$I_{90°}^{\text{off}}=\kappa n\frac{i}{e_0}lQ_T(3S\rightarrow 3D;90°) , \quad (5b)$$

where i is the electron current, e_0 is the elementary charge, l is the path length of an electron through the atom beam and κ is a detection constant that essentially includes a solid angle of observation, filter transmission, and photomultiplier sensitivity at 819 nm. When the laser is on, the $(1-f)n$ ground-state atoms are partially spin polarized, but as $Q_T(3S,M_S\rightarrow 3D;90°)$ does not depend on M_S the $Q_T(3S\rightarrow 3D;90°)$ are identical in Eqs. (5a) and (5b). On subtracting (5b) from (5a), we obtain

$$I_{\text{on}}-I_{\text{off}}=\kappa n\frac{i}{e_0}lf[Q_T(3P,M_L=1,M_S=\tfrac{1}{2}\rightarrow 3D;90°) - Q_T(3S\rightarrow 3D;90°)] . \quad (5c)$$

As will be discussed in a forthcoming publication,[14] the linear polarization of the $3D\rightarrow 3P$ radiation after electron excitation from the angular-momentum oriented P state does have an explicit dependence on M_S involving the exchange cross section, i.e., the polarization and $Q_T(3P,M_L=1,M_S=\frac{1}{2}\rightarrow 3D;90°)$ are M_S dependent.

The quantities $(I_{\text{on}}-I_{\text{off}})/i$ and I_{off}/i are measured as a function of electron energy, from 1–1000 eV. From Eqs. (5c) and (5b) these apparent excitation functions are proportional to $Q_T(3P,1,1/2\rightarrow 3D,90°)-Q_T(3S\rightarrow 3D;90°)$ and $Q_T(3S\rightarrow 3D,90°)$, respectively. To normalize these apparent excitation functions, we calculate $Q(i\rightarrow 3D)$ BA cross sections, correct these to $Q(i\rightarrow 3D,90°)=Q(i\rightarrow 3D)3/(3-P)$ using Born and Born-Ochkur approximation polarization, and add cascading that is also calculated using the BA. This cascading is a minor ($\sim$10%) correction, and its polarization produces a $\sim$10% correction to this correction, so this is neglected. This procedure yields BA values for $Q_T(i\rightarrow 3D,90°)$, and we normalize the data to this at $E=200$–1000 eV, where clear convergence of the experimental and theoretical energy dependence is obtained.

III. APPARATUS

In optical excitation function experiments dealing with excitation of ground-state atoms, the essential experimental criterion is to focus the electron beam at all energies through a fixed region of uniform atom beam density and optical detection sensitivity. In such experiments, variations of electron beam position or size with energy can therefore be tolerated to an extent determined by the design of atom beam and detection optics. For electron collisions with excited atoms, the electron beam must pass through a region of spatially homogeneous density of excited atoms. This is particularly important at low energies where electrons are prone to deflection by small residual electric and magnetic fields. Considerable care has therefore been taken to ensure such a spatially homogeneous excited atom region and that the entire electron beam traverses this region.

Figure 3 shows a diagram of the apparatus in the plane of electron and sodium beam. Electron and laser beam travel antiparallel to each other to intersect the sodium beam at right angles. Observation of the optically and collisionally excited fluorescence is made along the third, orthogonal axis. Figure 4 shows the apparatus schematically in the plane of atom beam and the axis of optical detection.

Electrons are produced by an indirectly heated oxide cathode, controlled by a grid, accelerated by anodes A_1 and A_2, and focused into the interaction region by a lens formed by elements A_2', V, and aperture 1. Except for the following, this gun has been described in Ref. 15. An opening at the end of the cup is provided for the incoming laser beam, but complete electron collection is achieved by using a reflector electrode as a last element. Keeping this element at a potential a few volts below cathode prevents

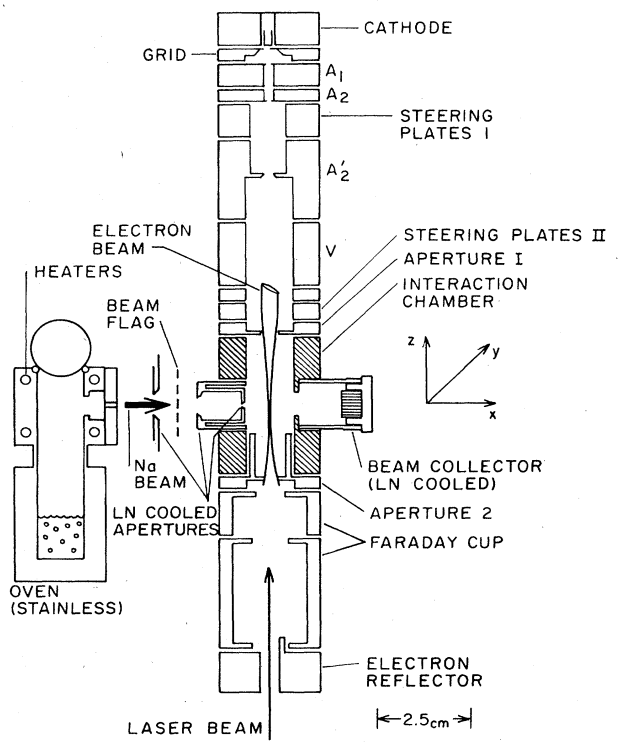

FIG. 3. Diagram to scale of the apparatus, in the (x-z) plane of the Na, electron, and laser beams.

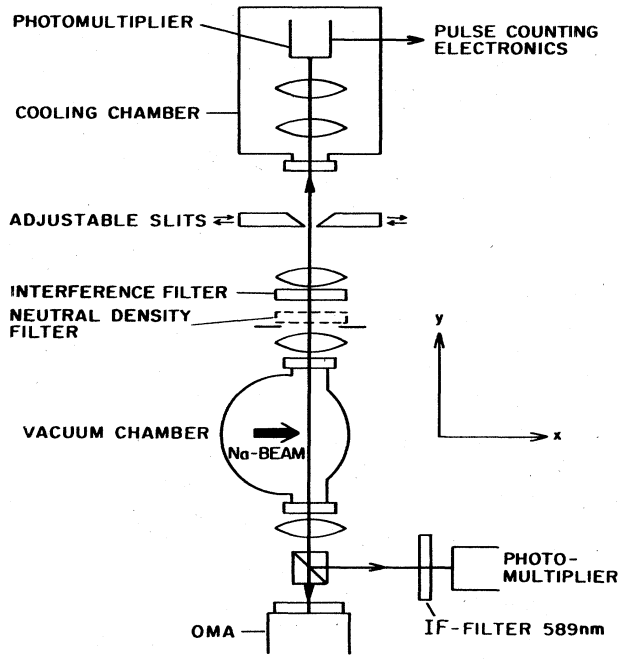

FIG. 4. Top view of the apparatus, in the $(x$-$y)$ plane of the Na beam and detection optics. The OMA (optical multichannel analyzer) was used to monitor the Na($3P$) spatial distribution, and the photomultiplier monitored the total Na($3P$) density.

electrons from traveling beyond the Faraday cup, and an asymmetric half cylinder on top of the reflector deflects the reflected electrons into the walls of the cup, preventing reflection back through the interaction chamber. This was verified by dividing the electron collector into segments and measuring the individual currents to each of them.

Two sets of electron beam steering elements are employed. The first, near the cathode, compensates for deviations from cylindrical symmetry within the electron gun. The second, close to the interaction chamber, does the same for the collision region.

The distance between cathode and grid has been decreased slightly compared to Ref. 15. This increased the current density at low energies, but sacrificed some current at higher energies.

Typically, the total electron current passing through the interaction chamber is 0.1—0.5 and 5—10 μA at 2 and 100 eV. That greater than 98% of this current transverses the optically excited regions of the atom beam at all relevant electron energies is established by the optical measurements described below. The apertures 1 and 2, before and after the interaction chamber, have a cup geometry to assist in electron collection, and their currents are used to give an indication of the beam size and direction. The currents to apertures 1 and 2 are typically 2% and 7% of the total current at 2 eV, and less than 0.04% at 100 eV. For low electron energies about 30% of the aperture-2 current is not collected, so a correction ($\sim$2%) is made in evaluating the total current.

The average energy of the electron beam is determined by measuring the $3S\rightarrow 3P$ apparent excitation function, and the energy distribution is measured at low average energies using aperture 2 and the cup as a retarding analyzer. This distribution is found to be equivalent to a thermal distribution with $kT=0.115$ eV and a FWHM of 0.29 eV, as expected for our oxide cathode source. Changes in the electron energy relative to the cathode voltage, which result from changes in the cathode and sodium build-up in the interaction chamber, are observed as changes in the apparent threshold for $3S\rightarrow 3P$ excitation. Corrections were made for these small energy shifts whenever they exceeded 0.01 eV.

The sodium beam is produced by a stainless steel oven with two heaters, typically with a reservoir region at $\sim$230°C. This results in an estimated sodium density in the interaction region of $\sim 10^9$ cm^{-3} and a dimer concentration of $\sim$0.1%.

Optical excitation of the atoms is accomplished by a frequency and intensity stabilized, cw dye laser of $\sim$1-MHz linewidth and typically $\sim$100 mW of power. Following standard practice[9] the laser beam is circularly polarized and tuned to the $3\,^2S_{1/2}$, $F=2\rightarrow 3\,^2P_{3/2}$, $F=3$ transition. In our apparatus it is expanded with two lenses and then circularly polarized inside the vacuum chamber with an air-spaced Glan-Thompson prism and a Fresnel rhomb. It optically pumps a major fraction of the atoms initially in $3\,^2S_{1/2}$, $F=2$ state into the $F=2$, $M_F=2$ level within $\sim$100 μm of entering the laser beam. Thereafter, 40—50% of these $F=2$, $M_F=2$ atoms are excited to the $3\,^2P_{3/2}$, $F=3$, $M_F=3$ state until the atoms leave the laser beam. The remaining fraction of the atoms initially in the $^2S_{1/2}$, $F=2$ state are inadvertently excited to the $3\,^2P_{3/2}$, $F=2$ state, due to the natural and Rabi line widths and residual Doppler width. From there they decay partially to $3\,^2S_{1/2}$, $F=1$ and remain there. The result in our apparatus was typically a beam $\sim$20% in the $3\,^2P_{3/2}$, $F=3$, $M_F=3$ state, $\sim$25% in the $3\,^2S_{1/2}$, $F=2$, $M_F=2$, and $\sim$55% in the $3\,^2S_{1/2}$, $F=1$ state. This leakage into $F=1$ can be decreased by allowing the initial optical pumping into $M_F=2$ to occur in the lower intensity periphery of a Gaussian laser beam, but in our apparatus the electron-optics aperatures truncated the laser beam edges.

The detection optics ($F/2.4$) images the interaction region into the plane of a pair of vertical slit edges, which are adjustable in the x (atom beam) direction, and this slit plane is then imaged onto the cathode of a cooled GaAs photomultiplier (see Fig. 4). These slits are used to scan the spatial distribution of the excited sodium atoms and the electron beam profile, as discussed below. The $3P$-$3S$ fluorescence is detected in the opposite direction for frequency-locking of the laser beam and monitoring the $3P$ density (Fig. 4).

IV. MEASUREMENTS

As was already pointed out, a very important experimental issue in measuring an electron excitation cross section from an excited atomic state is the overlap between electron beam and the region of homogeneously excited atoms. Thus we shall describe in detail the steps taken and control measurements performed to achieve satisfac-

tory overlap.

First, we ensured that the spatial distribution of the density of laser-excited atoms (Na*) and of the electron beam density were correctly observed. Thus, the sensitivity of the photomultiplier cathode, including the entire detection system, was measured and found to be constant within 4 mm along the x axis except for a few percent at the edges. Since the diameter of aperture 2, which defines the diameter of the laser beam in the interaction region, was 0.38 mm, the magnification of the optics was chosen to be 0.80, so that the entire region of laser-excited atoms was detected with homogeneous photocathode sensitivity.

Referring to Fig. 2, we wish to know the electron beam and Na* distributions along the directions of sodium beam (x axis) and of the optical detection (y axis). Two lenses expanded the laser beam to a half-width in the interation region that equaled the diameter of aperture 2. The Gaussian profile of the laser beam was thus cut off at the height of its half-width. The centering of the laser beam along the atom beam axis was accomplished by measuring the total fluorescence and the spatial distribution of the Na($3P$) atom fluorescence, scanning the adjustable slits (Fig. 4) that are in the image plane of the interaction region. The results of such a measurement are shown in Fig. 5, where it can be seen the data points form a smooth bell-shaped curve.

In order to interpret the data points in Fig. 5 note that this laser-excited fluorescence $I(x)$ is proportional to the Na($3P$) atom density Na*(x,y) integrated along y, i.e., the density along a chord of the excited cylinder. If this cylinder was homogeneously filled with Na($3P$) atoms, $I(x)$ would be proportional to $(r^2-x^2)^{1/2}$, where r is the radius of the cylinder (1.9 mm). (For the density of $\sim 10^9$ cm^{-3}, the atom beam is optically thin.) If this function is convoluted with the finite width (0.5 mm) of the scanning slit, one obtains the solid curve in Fig. 5. The good agreement with the data points shows that, as desired, the entire 3.8-mm region of atom beam illuminated by the laser has a very homogeneous Na($3P$) density. That this homogeneity is achieved despite the (truncated) Gaussian profile of the laser beam is, of course, due to the high degree of saturation of the $3\,^2S_{1/2}$, $F=2$, $M_F=2$ to $3P_{3/2}$, $F=3$, $M_F=3$ transition. As an indication of the level of saturation, when the laser intensity was reduced by 50%, the total fluorescence intensity decreased by $\sim 5\%$.

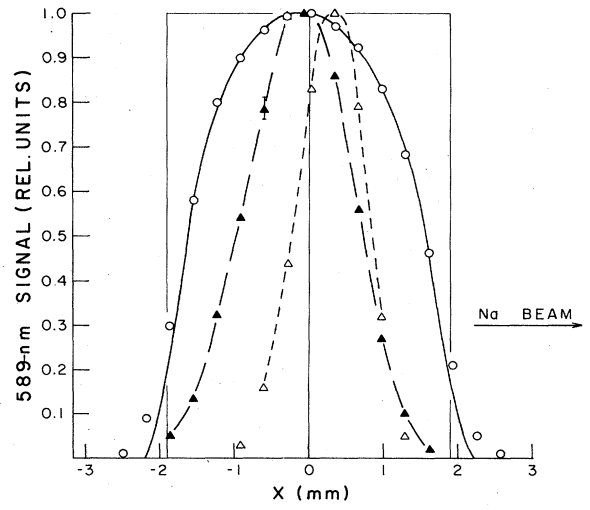

FIG. 5. Measured intensity as a function of slit position ("adjustable slits" in Fig. 4), corresponding to x position in the interaction volume (Fig. 2). Electron-beam excited 589 nm, resonance-line fluorescence is shown for a 2.2 eV (▲) and 100 eV (△) electron energy. Optically excited 589 nm fluorescence (○) is compared to that expected from a cylinder of uniform excitation (——).

Figure 5 also shows the x dependence of the electron-beam excited resonance-line (589 nm) fluorescence, for mean electron-beam energies E of 2.2 and 100 eV. Since the electron beam is cylindrically symmetric and centered in the y direction, it is clear that at these energies at least 98% of the electron beam traverses the 3.8-mm-diameter region of uniformly excited Na($3P$) atoms. These optical measurements confirmed that this situation also holds for all $E>2.2$ eV, but mean energies as low as 1.4 eV are important for the $3P\rightarrow 3D$ excitation. As this is far below the threshold for $3S\rightarrow 3P$ excitation, we relied on the aperture 1 and 2 currents to verify that the beam was correctly traversing the interaction region at these lower energies. Overall, our observations suggest an uncertainty in the cross section due to beam overlap of less than $\sim 3\%$ for $E>2.2$ eV, but increasing to 10% at $E=1.5$ eV.

Positioning of the laser in the y direction (Fig. 2) was accomplished by seeking the maximum total $3P$ fluorescence, while the electron beam was optimized in the y direction using aperture currents, occasionally supported by fluorescence measurements. We note that the major source of electron-beam deflection in the interaction chamber was a residual magnetic field (~ 30 mG) directed primarily along the y direction, due to the window opening in the otherwise μ-metal screened vacuum chamber. The resulting electron-beam deflection is primarily in the x direction, and was therefore optically detected and compensated by the steering unit II (Fig. 3).

The divergence half-angle of the laser and electron beam was less than 0.01 and 0.1 rad, respectively, so that the angle between both beams was less than 0.11 rad. This angle is significant because the $3P$ state is oriented along the laser beam axis, while the M_L and M_S dependent cross sections $Q(3P,M_L,M_S\rightarrow 3D,90°)$ must be referred to the electron velocity direction. We expect the effect of this $\Delta\theta\sim 0.1$ rad angular divergence to be less than a few percent because, by symmetry, it must introduce errors proportional to $\Delta\theta^2$. This is confirmed by BA calculations.[14]

The scheme outlined in Sec. II does not account for several types of background signals. The most important background contribution to the 819-nm signal was produced by surface scattering and Na fluorescence of 589-nm light, which illuminated surfaces and apparently produced broad-band surface fluorescence, a fraction of which was transmitted by our ~ 10-nm pass band 819-nm interference filter. This background increased slowly with beam-on time, implying a dependence on a Na layer (probably oxidized) on the walls of the interaction

chamber. To minimize this we chose the diameter of aperture 2 slightly smaller than that of aperture 1, but this background of typically ~ 1000 counts/sec was still one to two orders of magnitude higher than the typical $3D \rightarrow 3P$ fluorescence signal due to electron excitation of Na($3P$) to the $3D$ state. Consequently, rather long data accumulation was necessary (typically 24 h) for the low-energy region and the statistical uncertainty in the final $3P \rightarrow 3D$ cross section data is higher than one would expect for this experiment.

Other background signals, due to oven-light scattered-off surfaces, electron excitation of background gas, and photomultiplier dark current were much smaller than the above surface fluorescence signals. All of these backgrounds were measured and subtracted from the observed signals by separately switching the electron beam, Na beam flag, and laser beam on and off.

A. Normalization

From Eq. (5c), the measured $I_{on}-I_{off}$ intensity ($\Delta I_{90°}$) is proportional to $Q_T(3P,1,1/2\rightarrow 3D,90°)-Q_T(3S\rightarrow 3D,90°)$. Thus, we have used the Born approximation to calculate each of these cross sections and then normalized the high energy $\Delta I_{90°}$ data to their difference. This is done by calculating $Q(3P,M_L=1\rightarrow 3D)$ by BA, then calculating[14] $P(3P,1,1/2\rightarrow 3D)$ by Born-Ochkur approximation and taking $Q(3P,1,1/2\rightarrow 3D,90°)=Q(3P,1\rightarrow 3D)3/(3-P)$. This BA cross section and Born-Ochkur polarization are given in Table II. In each case the direct Born excitation cross section is multiplied by the polarization factor in Eq. (4), using Born-theory polarization, to obtain $Q(i\rightarrow 3D,90°)$, then the dominant cascade terms are added, as in Eq. (3), and assumed unpolarized. The resulting theoretical $Q_T(3P,1,1/2\rightarrow 3D,90°)$ $-Q_T(3S\rightarrow 3D,90°)$, multiplied by E, is plotted in Fig. 6. This data normalization corresponds to multiplying $\Delta I_{90°}(E)/\Delta I_{90°}(100\text{ eV})$ by $15.7\pi a_0^2$. For comparison, the BA cross section $Q_T(3P\rightarrow 3D)\times E$, without polarization of $M_L=1$ corrections, is also shown in Fig. 6.

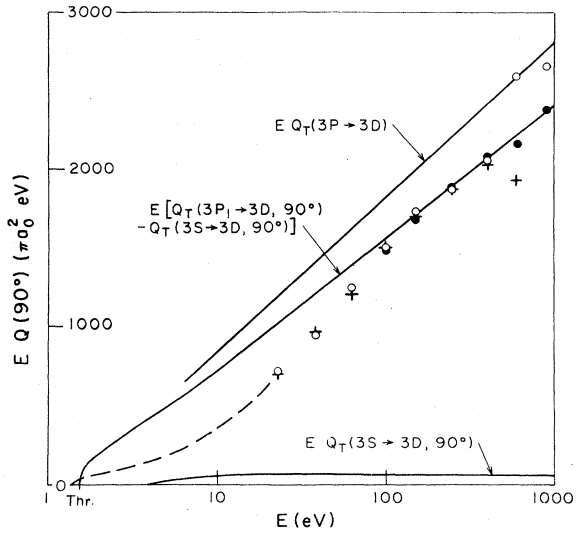

FIG. 6. The high-energy data and normalization procedure is shown; the solid lines correspond to Born approximation cross sections (including cascades). Different data runs are shown with different symbols. The data above 30 eV is shown as points, while that below 30 eV is represented by an average line (— — —).

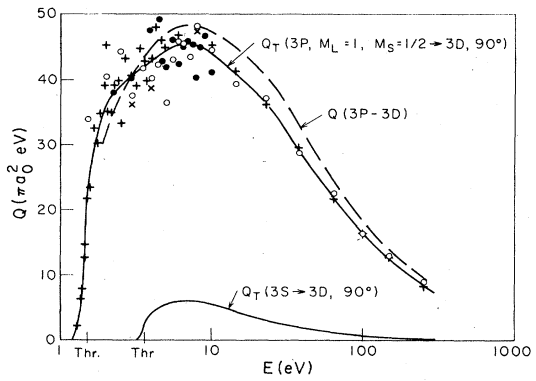

FIG. 7. Normalized $3P\rightarrow 3D$ cross section data, with a line drawn through the average, and an average of the $3S\rightarrow 3D$ data. Different data sets are shown with different symbols.

We have also measured the $3S\rightarrow 3D$ apparent optical excitation function, and from an independent high-energy normalization described below obtained $Q_T(3S\rightarrow 3D,90°)$ from this. A line equal to the average of these data is shown in Figs. 6 and 7. This measured $Q_T(3S\rightarrow 3D,90°)$ has been added to the $Q_T(3P,1,1/2\rightarrow 3D,90°)$ $-Q_T(3S\rightarrow 3D,90°)$ data $[\Delta I_{90°}(E)/\Delta I_{90°}(100\text{ eV})\times 15.7\pi a_0^2]$ to obtain the $Q_T(3P,1,1/2\rightarrow 3D,90°)$ points shown in Fig. 7. These points thus correspond to the measured $Q_T(3P,1,1/2\rightarrow 3D,90°)$, which is in absolute units as a result of the two high-energy normalizations. Uncertainties in the $Q_T(3S\rightarrow 3D,90°)$ data are very small, and have a negligible effect on the uncertainties in the points shown in Fig. 7. The $\sim 5\%$-rms fluctuations in the points below 10 eV in Fig. 7 are statistical, and within a few percent we find no indication of any structure in this

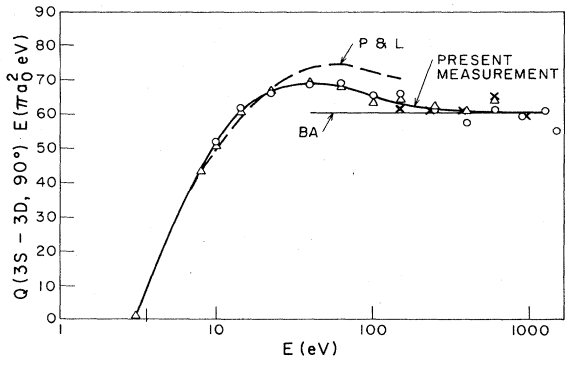

FIG. 8. High-energy $3S\rightarrow 3D$ total cross section data (points, with different data sets as different symbols), with an average line (solid) through our data, which is normalized as shown to the Born approximation (BA). The absolute measurement of the same quantity by Phelps and Lin is shown as a dashed line. The total cross section, including cascading and as observed at 90° is shown.

TABLE I. $3P \rightarrow 3D$ Born-approximation cross section.

E (eV)	$Q(3P \rightarrow 3D)$[a]	$Q(3P_1 \rightarrow 3D)$	$P(3P,1,1/2 \rightarrow 3D)$[b]	$Q_c(4F,5F,6F)$	$Q_T(3P,1,1/2 \rightarrow 3D,90°)$	$Q_T^{90°} \times E$
1.544	27.5	36.6	24.7	0	39.9	61.6
1.634	53.7	67.5	20.7	0	72.5	119
1.755	73.2	86.8	15.8	0	91.6	161
2.00	95.9	104.9	7.5	0	107.6	215
3.45	124.	119.8	−16.9	6.9	120.3	415
5.39	114.2	109.2	−27.7	6.6	106.6	574
9.26	90.9	87.8	−36.1	4.8	83.2	770
17.01	64.4	63.2	−42.6	2.9	58.3	991
32.50	42.0	41.7	−47.1	1.6	37.7	1225
63.50	25.9	26.0	−50.5	0.85	23.1	1467
113.5	16.62	16.78	−52.7	0.49	14.8	1675
227.0	9.58	9.73	−54.8	0.24	8.47	1923
605.3	4.27	4.36	−57.0	0.09	3.76	2273
1513.0	1.96	2.01	−58.5	0.04	1.72	2600

[a]All cross sections are in units of πa_0^2.
[b]Born-Ochker approximation is used for $E < 10$ eV. Percent polarization is indicated.

region. Thus, we have drawn an average line through the $Q_T(3P,1,1/2 \rightarrow 3D,90°)$ data in Fig. 7 to indicate this.

A polarization correction, cascade correction, and relation between $Q(3P,1 \rightarrow 3D)$ and $Q(3P \rightarrow 3D)$ are needed to obtain the direct $3P \rightarrow 3D$ cross section from the data in Fig. 7. Although the BA is not accurate below ~ 100 eV (see Fig. 6), we can use it to obtain an estimate of this ratio, $Q(3P \rightarrow 3D)/Q(3P,1 \rightarrow 3D)$, and we can use the Born-Ochkur approximation[14] for P in the polarization correction $(3-P)/3-Q(3P,1 \rightarrow 3D)/Q(3P,1,1/2 \rightarrow 3D,90°)$. These values are given in Table I, where columns 2 and 6 contain the calculated $Q(3P \rightarrow 3D)$ and $Q_T(3P,1,1/2 \rightarrow 3D,90°)$. Thus, to provide an estimate of the $Q(3P \rightarrow 3D)$ implied by our $Q_T(3P,1,1/2 \rightarrow 3D,90°)$ data, we multiply the solid line in Fig. 7 by ratio of column 2 to column 6, obtaining the dashed line in Fig. 7. At energies above ~ 4 eV this estimate should be reasonably accurate, as the size of the difference is fairly minor.

In Fig. 8 the high-energy $Q_T(3S \rightarrow 3D,90°)$ data, taken with the laser off, are plotted as $Q \times E$ versus $\ln E$. This has been normalized in the high-energy limit to the BA value of $Q_T(3S \rightarrow 3D,90°)$, as indicated by the average line drawn through the data. Table II indicates how this BA result is obtained from BA cross sections. The individual data points below 6 eV are shown in Fig. 9, and only an average line through these is shown in Fig. 8. The type of energy dependence seen here is the same as that reported for lithium $2S \rightarrow nD$ cross sections.[16] For ease of comparison, the average cross sections from our data, after normalization, are also given in Table III.

The threshold behavior of the $Q_T(3P,1,1/2 \rightarrow 3D)$ and $Q_T(3S \rightarrow 3D)$ cross sections is shown in Fig. 9, where it is compared to previously reported[15,17,18] $3S \rightarrow 3P$ cross sections. The most distinctive feature of these data is the very rapid onset of the $3P \rightarrow 3D$ and $3S \rightarrow 3D$ cross sections. For comparison, the Faraday cup current as a function of cup voltage, equivalent to a step-function cross section convoluted with our electron-energy distribution, is shown in the figure as solid lines shifted to the thresholds. Comparing this to the data, it is apparent

TABLE II. $3S \rightarrow 3D$ Born-approximation cross sections.

E (eV)	$Q(3S \rightarrow 3D)$[a]	$P(3D \rightarrow 3P)$	$Q_c(4F,5F,6F)$	$Q_c(4P)$	$Q_T(3S \rightarrow 3D)$	$Q_T^{90°}(3S \rightarrow 3D)$
3.69	1.94	40.	0	0	1.94	2.24
3.91	3.59	39.4	0	0.03	3.62	4.17
4.20	4.61	38.6	0	0.05	4.66	5.35
4.77	5.48	36.6	0.19	0.06	5.73	6.53
5.93	5.75	34.1	0.37	0.06	6.18	6.97
8.25	5.13	29.8	0.35	0.05	5.52	6.13
12.9	3.82	22.7	0.25	0.04	4.11	4.45
22.1	2.44	12.2	0.15	0.02	2.62	2.73
40.7	1.403	0.1	0.085	0.014	1.50	1.50
77.7	0.756	−11.5	0.045	0.008	0.808	0.778
151.8	0.393	−18.1	0.023	0.004	0.420	0.396
271	0.221	−21.2	0.013	0.003	0.237	0.221
543	0.1112	−23.3	0.0064	0.0013	0.119	0.110
904	0.0668	−24.1	0.0038	0.0008	0.0714	0.0661
2530	0.0239	−24.9	0.0014	0.0003	0.0256	0.0236

[a]All cross sections are in units of πa_0^2.
[b]Born-Ochkur polarization, in percent, is reported.

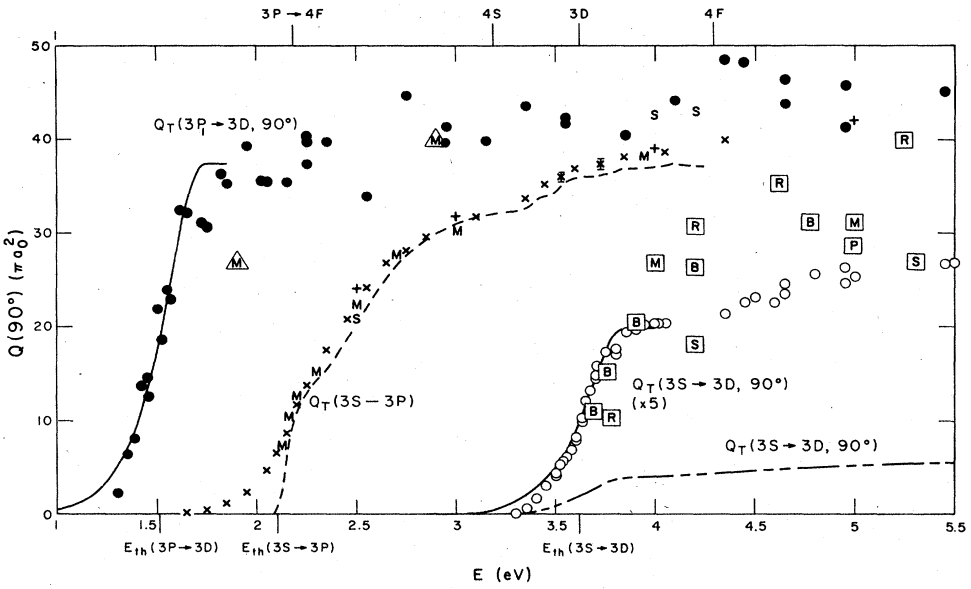

FIG. 9. Measured threshold behavior of the $3S\rightarrow 3P$ (×, +, and — — —), $3S\rightarrow 3D$ (○ plotted ×5 and — · — ·) and $3P\rightarrow 3D$ (●) cross sections, compared to theories (letters). The present $3S\rightarrow 3P$ cross section data (×) is compared to that of Enemark and Gallagher (+) and Haffner and Kleinpoppen (— — —). The solid lines are the cup current as a function of cup voltage, representing the electron energy distribution for a step-function cross section, offset to the $3P\rightarrow 3D$ and $3S\rightarrow 3D$ thresholds to compare to the measurements. Calculated cross sections by Moores and Norcross (M) and by Shuker (S) are compared to the $3S\rightarrow 3P$ measurements. A value of $55\pi a_0^2$ at 5 eV, calculated by Phelps and Lin, is just off the graph and not shown. $3D$ state cascading to $3P$ has been added to these calculated $3S\rightarrow 3P$ cross sections, for direct comparison to the Q_T data. The $Q(3P\rightarrow 3D)$ calculated by Moores and Norcross (△) is compared to the present $Q_T(3P_1\rightarrow 3D, 90°)$ data (●). Calculations by Moores, Norcross and Sheorey □, Phelps and Lin □, Shuker □, Rudge □, and Born approximation □, are compared to the present $Q_T(3S\rightarrow 3D, 90°)$ data (○). All of the theoretical $Q(3S\rightarrow 3P)$ have been corrected to $Q(3S\rightarrow 3P, 90°)$, using $3D\rightarrow 3P$ polarization measured by Phelps and Lin.

that, within the energy resolution of our experiment, these $Q_T(3P,1,1/2\rightarrow 3D)$ and $Q_T(3S\rightarrow 3D)$ are essentially step functions at threshold. The $Q_T(3S\rightarrow 3P)$ also rises very rapidly above threshold compared to many other measured cross sections, but as can be seen it is much less rapid than the $3P,1,1/2\rightarrow 3D$ and $3S\rightarrow 3D$ cross sections. (The $3P,1,1/2\rightarrow 3D$ and $3S\rightarrow 3D$ cross sections convoluted with our energy resolution reach 75% of their initial peak value in Fig. 9 at ~0.1 eV above threshold, while this requires ~0.5 eV for the $3S\rightarrow 3P$ cross section.)

TABLE III. Normalized, measured cross sections.

E (eV)	Average $Q_T(3P_1\rightarrow 3D,90°)$	Average $Q_T(3S\rightarrow 3D,90°)$
2.0	34	0
2.5	37	0
3.0	39	0
4.0	41	4.0
5.0	42	5.1
7	43	5.5
10	42	5.0
20	36	3.27
50	24	1.37
100	15.6	0.65
300	6.7	0.203
1000	2.45	0.060

V. COMPARISON

The $Q_T(3S\rightarrow 3D,90°)$ measured here are compared to the measurements of Phelps and Lin[18] in Fig. 8, where it can be seen that they are in agreement within the experimental uncertainties, although there is a slight difference in shape from 20—150 eV. The uncertainty in our measurement is estimated at 5—10%, while an uncertainty given in Ref. 18 is 10%.

Except at threshold, the general shape of the cross section for the electric-dipole-allowed $3P\rightarrow 3D$ transition, relative to the BA, is characteristic of the resonance-line ($nS\rightarrow nP$) excitation cross sections.[19,20] For example, convergence to the BA within ~10% occurs at ~50 times the threshold energy, and in the peak region of the cross section the BA overestimates by a factor of 2—3. It is well known that the lack of normalization in the BA causes most of this error.

The primary calculation of cross sections for the low-energy region is the four-state close-coupling calculation of Moores, Norcross, and Sheorey.[21] They were optimizing their calculations with regard to the $3S\rightarrow 3P$ excitation, but they included $3S\rightarrow 3D$ and $3P\rightarrow 3D$ results. These are shown in Fig. 9 (labeled M) for all three excitations. It can be seen that their results are within 5—10% agreement with the experiments for the $3S\rightarrow 3P$ excitation. [Here we have added the experimental $Q_T(3P\rightarrow 3D)$ to their calculated $Q(3S\rightarrow 3P)$ at 4 eV, so that the theoretical point can be compared directly to the measure-

ments, which include 100% cascading from the $3D$ state.] The Moores *et al.* results for $Q(3S \rightarrow 3D)$ are about 25% high [here cascading measured by Phelps and Lin[18] has been added to the calculation for comparison to the $Q_T(3S \rightarrow 3D)$ data shown in Fig. 9].

In order to compare the close-coupling results for $Q(3P \rightarrow 3D)$, done at 1.9 and 2.9 eV, to the measurements of $Q_T(3P_1 \rightarrow 3D, 90°)$, the latter must be corrected for unknown polarization, cascading, and $Q(3P_1 \rightarrow 3D)/Q(3P \rightarrow 3D)$ ratio. A guess at these corrections would lower the data by 20—30% at both energies, leading to reasonable agreement with the theory (see Fig. 9). However, theoretical or experimental values for the above corrections are needed for a definitive comparison, as are theoretical values close to threshold to explain the very rapid rise in the cross section.

Two other close-coupling calculations have reported only the $3S \rightarrow 3P$ and $3S \rightarrow 3D$ cross sections. That of Korff, Chung, and Lin,[22] which includes many states to optimize the intermediate-energy regions but neglects exchange, has already been compared by Phelps and Lin[18] to their measured, cascade-corrected $3S \rightarrow 3D$ cross section. The lowest-energy calculated point, at 5 eV, is shown in Fig. 9, where it is $\sim 20\%$ above our measured value, after making the cascade correction given by Phelps and Lin. Shuker and Azar[23] have recently carried out a three-state close-coupling calculation optimized for the $3S \rightarrow 3P$ cross section. As seen in Fig. 9, their $3S \rightarrow 3P$ results are close to the experiment at 2.5 eV, and after adding cascading about 15% high at ~ 4 eV.

VI. CONCLUSIONS

The electron collisional excitation of the $3D$ state of the Na represents a more severe problem in electron-collision theory than the $3S \rightarrow 3P$ excitation that has been studied for many years. As can be seen from the Na energy levels in Fig. 1, the $3D$ state is only 0.1 eV from the $4P$ state, to which it can be strongly coupled at long range. Furthermore, for electron energies ≥ 0.1 eV above the $3D$ threshold energy the $3P$, $4S$, $3D$, and $4P$ channels are all open, within 0.8 eV, another five channels are open. Of course, higher-state excitations become a multistate problem even more quickly. In spite of this level of complication, when viewed from the standpoint of close-coupling theory, the $3S \rightarrow nL$ excitation cross sections fit a simple pattern, from a few times the excitation energy to high energies, as already shown by Phelps and Lin[18] and Zajonc and Gallagher.[16]

The threshold behavior for higher-state excitation has not been carefully studied, and here we have shown that both the $3S \rightarrow 3D$ and $3P \rightarrow 3D$ cross sections have very rapid onsets, rising to $\sim 75\%$ of their peak values within 0.1 eV or less. This is much more rapid than has normally been observed for spin-allowed excitation cross sections, and it is even more unusual for a dipole-allowed transition. Johnston and Burrow[24] have reported sharp scattering resonances in this region, and these may be closely related. From the common behavior of these $3S \rightarrow 3D$ and $3P \rightarrow 3D$ onsets, this appears to be an "upper-state" effect. If the upper state does dominate, then we would expect the steepness of the cross section onset to increase as the upper-state binding decreases, because the threshold energy from nearby levels also decreases. However, negative ion states and resonances may play a major role here, and more data and theory for other transitions are needed to make any meaningful generalization of this interesting and somewhat unexpected feature.

ACKNOWLEDGMENTS

We wish to thank Richard Dang for assistance in the initial stages of this experiment. One of us (B.S.) would like to thank the Deutsche Forschungsgemeinschaft (Bonn, Germany), and the U.S. Army Research Office, Department of the Army (Durham, NC) for support during this work. Support from the National Science Foundation under Grant No. PHY-82-00805 is also gratefully acknowledged.

*Present address: Physics Department, New York University, 4 Washington Place, New York, NY 10003.

[1]M. R. Flannery and K. J. McCann, J. Phys. B **12**, 427 (1979).
[2]C. S. Gee, I. C. Percival, J. G. Lodge, and D. Richards, Mon. Not. R. Astron. Soc. **175**, 209 (1976).
[3]L. Vriens and A. H. M. Smeets, Phys. Rev. A **22**, 940 (1980).
[4]R. Shuker, A. Gallagher, and A. V. Phelps, J. Appl. Phys. **51**, 1306 (1980).
[5]G. Himmel and F. Pinnekamp, J. Phys. B **10**, 1457 (1977).
[6]J. F. Delpeche, J. Boulmer, and F. Devos, Phys. Rev. Lett. **39**, 1400 (1977); F. Devos, J. Boulmer, and J. F. Delpeche, J. Phys. (Paris) **40**, 215 (1979).
[7]J. E. M. Goldsmith and J. E. Lawler, Cont. Phys. **22**, 235 (1981).
[8]A. Ben-Amar, G. Erez, and R. Shuker, J. Appl. Phys. **54**, 3688 (1983).
[9]I. V. Hertel and W. Stoll, J. Phys. B **7**, 570 (1974); **7**, 583 (1974); H. W. Herman and I. V. Hertel, Z. Phys. **A307**, 89 (1982).
[10]G. F. Hanne, C. Szmythowski, and M. van der Wiel, J. Phys. B **15**, L109 (1982).
[11]D. F. Register, S. Trajmar, G. Csanak, S. W. Jensen, M. A. Fineman, and R. T. Poe, Phys. Rev. A **28**, 151 (1983).
[12]B. Jaduszliwer, G. F. Shen, J.-L. Cai, and B. Bederson, Phys. Rev. A **31**, 1157 (1985), and references therein.
[13]B. L. Moiseiwitsch and S. J. Smith, Rev. Mod. Phys. **40**, 238 (1968). Note erratum concerning polarization in Rev. Mod. Phys. **41**, 574E (1969).
[14]B. Stumpf (unpublished).
[15]E. A. Enemark and A. C. Gallagher, Phys. Rev. A **6**, 192 (1972).
[16]A. Zajonc and A. Gallagher, Phys. Rev. A **20**, 1393 (1979).
[17]H. Hafner and H. Kleinpoppen, Z. Phys. **198**, 315 (1967).
[18]J. O. Phelps and C. C. Lin, Phys. Rev. A **24**, 1299 (1981).
[19]S. T. Chen and A. C. Gallagher, Phys. Rev. A **17**, 551 (1978).
[20]S. T. Chen and A. C. Gallagher, Phys. Rev. A **14**, 593 (1976).

[21]D. L. Moores and D. W. Norcross, J. Phys. B 5, 1482 (1972); D. L. Moores, D. W. Norcross, and V. B. Sheorey, J. Phys. B 7, 371 (1974).
[22]D. F. Korff, S. Chung, and C. C. Lin, Phys. Rev. A 7, 545 (1973).
[23]R. Shuker and Z. Azar (private communication).
[24]A. R. Johnston and P. D. Burrow, Bull. Am. Phys. Soc. 28, 798 (1983).